

Origin of the Spin density wave instability in $A\text{Fe}_2\text{As}_2$ ($A=\text{Ba}, \text{Sr}$) as revealed by optical spectroscopy

W. Z. Hu, J. Dong, G. Li, Z. Li, P. Zheng, G. F. Chen, J. L. Luo, and N. L. Wang
*Beijing National Laboratory for Condensed Matter Physics,
Institute of Physics, Chinese Academy of Sciences, Beijing 100190, China*

We performed optical spectroscopy measurement on single crystals of BaFe_2As_2 and SrFe_2As_2 , the parent compounds of FeAs based superconductors. Both are found to be quite metallic with fairly large plasma frequencies at high temperature. Upon entering the spin-density-wave (SDW) state, formation of partial energy gaps was clearly observed with the presence of surprisingly two different energy scales. A large part of the Drude component was removed by the gapping of Fermi surfaces (FS). Meanwhile, the carrier scattering rate was even more dramatically reduced. We elaborate that the SDW instability is more likely to be driven by the FS nesting of itinerant electrons rather than a local-exchange mechanism.

PACS numbers: 74.25.Gz, 74.25.Jb, 74.70.-b

The recent discovery of superconductivity with transition temperature T_c above 50 K in $\text{RFeAsO}_{1-x}\text{F}_x$ ($\text{R}=\text{La}, \text{Ce}, \text{Sm}, \text{Pr}, \text{Nd}, \text{etc}$) has created tremendous interests in the scientific community.[1, 2, 3, 4]. Those compounds crystallize in a tetragonal ZrCuSiAs -type structure, which consists of alternate stacking of edge-sharing Fe_2As_2 tetrahedral layers and R_2O_2 tetrahedral layers along c -axis. The parent compound LaFeAsO itself is not superconducting but shows strong anomalies near 150 K in resistivity, magnetic susceptibility, specific heat, etc. Based on experimental observations and first principle calculations, it is suggested that the ground state is a spin-density-wave (SDW) ordered state with a stripe-type (or collinear) spin configuration.[5] The predicted magnetic structure was confirmed by subsequent neutron diffraction experiment, although the neutron data indicated that a subtle structural distortion occurs first near 150 K, and the SDW long range order establishes at a slightly lower temperature.[6] With fluorine doping, the SDW order is suppressed and superconductivity emerges.[2, 5] The very closeness of the superconducting phase to the SDW instability suggests that the magnetic fluctuations play a key role in the superconducting pairing mechanism.

Investigating the origin of the antiferromagnetic (AFM) SDW instability in the parent compound is an essential step towards understanding the mechanism of superconductivity in doped systems. The stripe-type AFM order was first suggested to result from the nesting between the hole and electron Fermi surfaces (FS) of itinerant electrons.[5] Alternatively it was proposed that the superexchange interaction mediated through the off-plane As atom plays a key role in the spin configuration formation.[7, 8, 9, 10, 11, 12] A stripe-type AFM would arise when the next nearest neighbor exchange becomes larger than half of the nearest neighbor exchange interaction. Whether an itinerant picture or a local superexchange mechanism should be taken as a starting approach becomes one of the most important issues for

those systems.[13]

Very recently, it is found that the ThCr_2Si_2 -type ternary iron arsenide BaFe_2As_2 , which contains identical edge-sharing Fe_2As_2 tetrahedral layers as in LaFeAsO , exhibits a similar SDW instability at 140 K.[14] It is therefore suggested that BaFe_2As_2 could serve as a new parent compound for ternary iron arsenide superconductors. Shortly after that, the superconductivity with $T_c=38$ K was found in K-doped BaFe_2As_2 , which was suggested to be a hole-doped iron arsenide superconductor.[15] The SDW instability was also found in SrFe_2As_2 with a higher transition temperature near 200K,[16, 17] while K-doping again introduces the superconductivity with $T_c\sim 38$ K.[17] For both parent compounds, the same stripe-type AFM order was confirmed by neutron experiments.[18, 19] A great advantage of those ternary iron arsenide compounds is that it is much easier to grow large size single crystals.[20]

In this letter we present optical study on both BaFe_2As_2 and SrFe_2As_2 single crystals. We find the undoped compounds of Fe-pnictides are quite metallic with rather high plasma frequencies, $\omega_p \geq 1.5$ eV. Upon entering into the SDW state, formation of energy gaps was clearly observed. Surprisingly, the optical measurement revealed two distinct energy scales in the gapped state. Associated with the gapping of the FS, a large part of Drude component is removed, meanwhile the carrier scattering rate shows even steeper reduction. Beyond the character energy for SDW gap, another spectral suppression in $\text{R}(\omega)$ which covers a much higher energy scale is present even above SDW transition temperature. The physical implications of those results were discussed. Our study favors an itinerant electron approach for the driving mechanism of SDW instability.

Single crystals of BaFe_2As_2 and SrFe_2As_2 (space group $I4/mmm$) were grown from the FeAs flux method.[21] The plate-like crystals could be easily cleaved, resulting in very shiny surface. The T-dependent dc resistivity was measured by the four contact technique in a Quan-

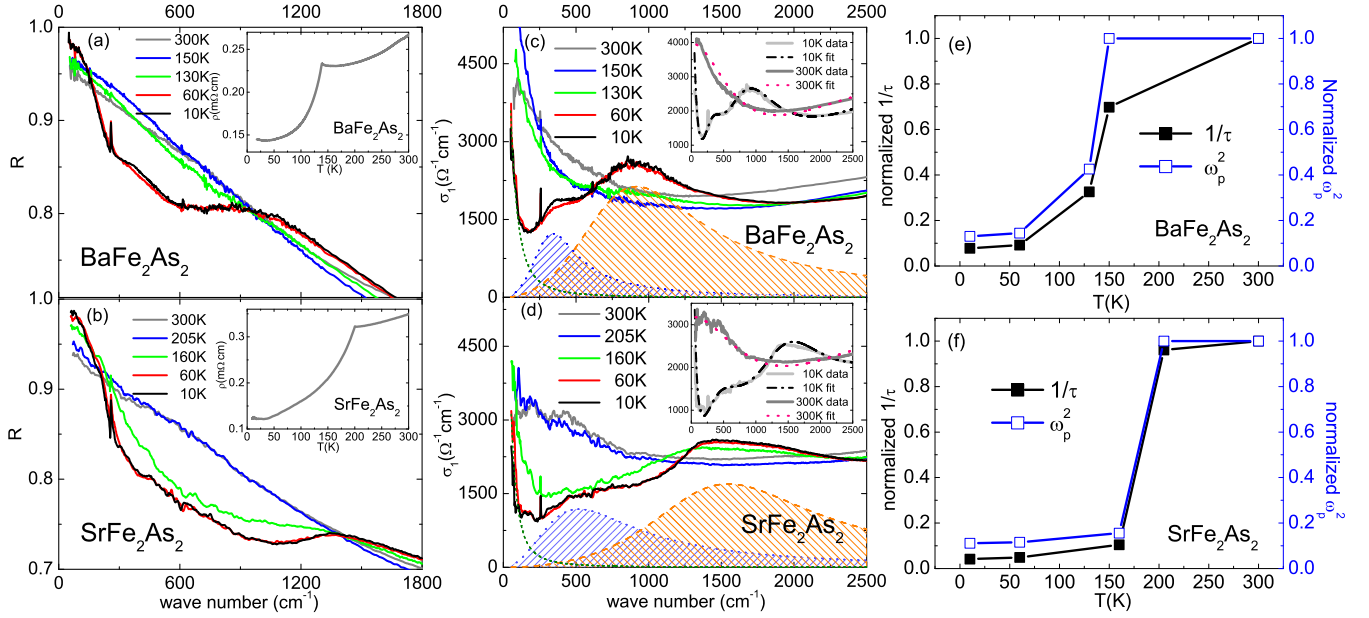


FIG. 1: (Color online) Left panel: $R(\omega)$ for (a) BaFe_2As_2 and (b) SrFe_2As_2 below 1800 cm^{-1} . Inset: the dc resistivity. Middle panel: $\sigma_1(\omega)$ for (c) BaFe_2As_2 and (d) SrFe_2As_2 below 2500 cm^{-1} . The Drude term (short dash green line) and the first two Lorentz peaks abstracted from a Drude-Lorentz fit for $T=10 \text{ K}$ is shown at the bottom. Inset: experimental data and the fit for $T=10$ and 300 K below 2500 cm^{-1} . Right panel: normalized $1/\tau$ (black) and ω_p^2 (blue) for (e) BaFe_2As_2 and (f) SrFe_2As_2 .

tum Design PPMS. As shown in Fig. 1, both samples show metallic T -dependence in the whole measurement temperature range. The resistivity drops sharply at 138 K and 200 K for BaFe_2As_2 and SrFe_2As_2 , respectively, which are ascribed to the formation of SDW order.

The optical reflectance measurements were performed on a combination of Bruker IFS 66v/s, 113v and a grating-type spectrometers on newly cleaved surfaces (ab-plane) for AFe_2As_2 ($A=\text{Ba}, \text{Sr}$) single crystals in the frequency range from 40 to 50000 cm^{-1} . An *in situ* gold and aluminium overcoating technique was used to get the reflectivity $R(\omega)$. The real part of conductivity $\sigma_1(\omega)$ is obtained by the Kramers-Kronig transformation of $R(\omega)$.

The main panels of Fig. 1 (a) and (b) focus on the low frequency $R(\omega)$ up to 1800 cm^{-1} . For both compounds, $R(\omega)$ exhibits a metallic response, and approaches to unity at zero frequency. The most prominent feature is a substantial suppression in $R(\omega)$ for $T < T_{SDW}$, which is a strong optical evidence for the formation of energy gaps. The low- ω reflectance increases faster towards unity at zero frequency than those at high T . As a consequence, one can see a rather sharp low- ω reflectance edge. This indicates clearly that the Fermi surfaces are only partially gapped and the compounds are still metallic below T_{SDW} . The change of $R(\omega)$ from a overdamped linear- ω dependent behavior to a well-defined reflectance edge upon cooling the sample into SDW ordered state immediately suggests a dramatic reduction of the carrier scattering rate, while its low-energy location implies a considerable reduction of carrier density. A quantitative

analysis will be given below. It is noted that the low- T $R(\omega)$ displays an almost linear- ω dependence over a certain frequency range below the suppression. This special shape of the suppression leads to the two-peak structure in optical conductivity.

The middle panels of Fig. 1 show the conductivity spectra $\sigma_1(\omega)$ below 2500 cm^{-1} . The Drude-like conductivity can be observed for all spectra at low frequencies. For BaFe_2As_2 ($T_{SDW}=138 \text{ K}$), a weak feature around 890 cm^{-1} develops for $T=130 \text{ K}$ in $\sigma_1(\omega)$, then the spectra are severely suppressed at low frequencies for 60 K and 10 K , resulting in a pronounced double-peak character at 360 and 890 cm^{-1} . Associated with the low- ω reflectance edge, a very sharp and narrow Drude component emerges below the double peaks. Very similar features can be seen for SrFe_2As_2 crystal, but the double peak features appear at higher energies, *i.e.* 500 and 1360 cm^{-1} , being consistent with the higher T_{SDW} for SrFe_2As_2 . The electrodynamics of broken symmetry ground states, such as the superconducting and density wave states, have been well explored and understood. Due to different coherence factors, a density wave state behaves different from an s-wave superconductor at the gap frequencies in optical conductivity. In an s-wave superconducting state at $T = 0$, the absorption smoothly rises at the gap frequency, while for a density wave state, a sharp maximum appears in conductivity at the gap frequency.[22, 23] Based on those studies, we can identify the double peak energies as the two SDW gaps. The observation of two distinct SDW gaps should be associated

with different Fermi surfaces, and reflect the multi-band property in FeAs based compound. From the gap values and SDW transition temperatures, we obtained the ratio of $2\Delta/k_B T_{SDW} \approx 3.5-3.6$ for the smaller gap, and 9-9.6 for the larger gap for the two compounds. The smaller gap coincides roughly with the gap value expected by the conventional BCS relation, while the large one is very different. Similar two-gap behaviors were also found in optical measurement for the itinerant SDW metal Cr.[24].

Due to the presence of two different gap values in the SDW ordered state, direct information on where the FS sheets are gapped is highly desired. Very recently, two angle resolved photoemission spectroscopy (ARPES) investigations on BaFe₂As₂ single crystals were reported, however, they yielded completely different results from optics. Yang *et al.*[25] reported a complete absence of gap opening for all bands at the Fermi level. Liu *et al.*[26] observed a small circular-shaped hole pocket centered at Γ and a large electron pocket at X point below T_{SDW} (at 100 K) on BaFe₂As₂ which matches well with full-potential linearized plane wave calculations. However, the gap opening is also absent in this work. Apparently the available ARPES data are in sharp contrast to our results. We emphasize that optical measurement is a bulk probe, while ARPES measurement strongly depends on the surface quality. We also noted that the large area of FS seen by Liu *et al.* below T_{SDW} is incompatible to the quantum oscillation experiment which reveals a rather small residual FS (occupying only 2% of the Brillouin zone).[27] More experiments are needed to resolve the inconsistency.

It is well-known that the low- ω Drude component comes from the itinerant carrier contribution. The Drude spectral weight determines the ω_p^2 (ω_p is the plasma frequency), which is proportional to n/m_{eff} (where n is the carrier density, m_{eff} is the effective mass); while its width reflects the carrier scattering rate $1/\tau$. To qualitatively analyze the T-evolution of the free-carrier component, we fit the optical response by the Drude-Lorentz model for the whole T and frequency range.

$$\epsilon(\omega) = \epsilon_\infty - \frac{\omega_p^2}{\omega^2 + i\omega/\tau} + \sum_{i=1}^N \frac{S_i^2}{\omega_i^2 - \omega^2 - i\omega/\tau_i}. \quad (1)$$

Here, ϵ_∞ is the dielectric constant at high energy, the middle and last terms are the Drude and Lorentz components, respectively. We use one Drude component for the free-carrier response, and several Lorentz terms to fit the high frequency $\sigma_1(\omega)$, including the double-peak SDW gap below T_{SDW} , a pronounced mid-infrared feature near 5000 cm^{-1} (Fig. 2 (b)), and some Lorentz components above 16000 cm^{-1} for interband transitions. The experimental $\sigma_1(\omega)$ data could be well reproduced by the fit (see the insets of Fig. 1 (c) and (d)).

We are now mainly concerned with the evolution of the itinerant carriers. For BaFe₂As₂, the plasma frequency

$\omega_p \approx 12900 \text{ cm}^{-1}$ and scattering rate $1/\tau \approx 700 \text{ cm}^{-1}$ at 300 K reduce to 4660 cm^{-1} and 55 cm^{-1} at 10 K, respectively. For SrFe₂As₂, $\omega_p \approx 13840 \text{ cm}^{-1}$ and $1/\tau \approx 950 \text{ cm}^{-1}$ at 300 K reduce to 4750 cm^{-1} and 40 cm^{-1} at 10 K, respectively. Figure 1 (e) and (f) shows the variations of $1/\tau$ and ω_p^2 with temperature for the Drude term. Both parameters are normalized to their 300 K value. Provided the effective mass of itinerant carriers does not change with temperature, then the residual carrier density is only 12% of that at high temperature for both compounds. This means that roughly 88% of FS is removed by the gapping associated with SDW transitions. On the other hand, the scattering rate was reduced by about 92-96%. Therefore, the opening of the SDW partial gap strongly reduces the scattering channel, leading to a metallic behavior with enhanced dc conductivity in the gapped state.

The above observations have important implication for the driving mechanism of SDW instability. As mentioned above, the key issue here is whether an itinerant picture based on FS nesting or a local superexchange mechanism is a proper approach. Our optical studies clearly demonstrate that the parent compound has a high itinerant carrier density with the plasma frequency a bit higher than 1.5 eV before SDW transition, and is rather metallic both above and below SDW ordering temperatures. Furthermore, the partial gap openings below SDW ordering temperatures are consistent with the expectation of nesting scenario where the temperature dependence of the gap should resemble that of BCS theory. On this basis, we think that the local picture is less favored, and the itinerant scenario provides more reasonable explanation for the driving mechanism.

Besides the dramatic spectral change at low frequencies, both compounds display very similar and pronounced spectral feature at the mid-infrared region. Take BaFe₂As₂ as an example, the mid-infrared component takes up a large spectral weight as shown in the inset of Fig. 2 (b). The peak at such a high energy is usually ascribed to the interband transition. However, a puzzling problem is that the spectra *below* the peak energy exhibit an apparent T-dependence that $R(\omega)$ is obviously suppressed with decreasing T below 5000 cm^{-1} (Fig. 1 (a)). Such a gap-like feature is present at all temperatures. Indeed, an analysis for the spectral weight in $\sigma_1(\omega)$ revealed that the suppressed spectral weight below 5000 cm^{-1} is transferred to higher energies. Figure 2 (c) plots the spectral weight for $\sigma_1(\omega)$ at 10 and 300 K. Below 200 cm^{-1} , the narrowing Drude peak with decreasing T (see the extrapolation data in Fig. 2 (b)) yields a growing dc conductivity thus a larger low frequency spectral weight for T=10 K. Above 200 cm^{-1} , the SDW double-gap develops which strongly reduces the low T Drude weight, leading to the first suppression below 1000 cm^{-1} in Fig. 2 (c). The lost Drude weight fills into the SDW double-peak, and the total spectral weight is almost recovered

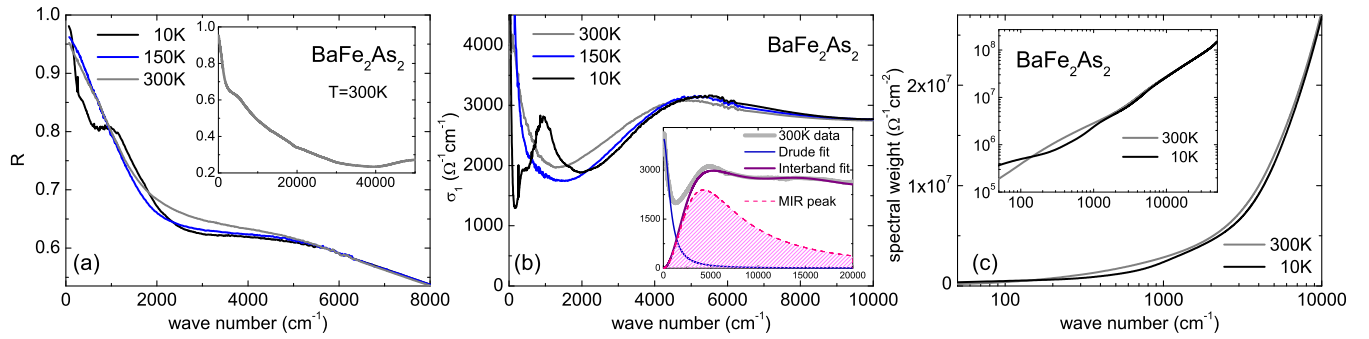


FIG. 2: (Color online) (a) $R(\omega)$ for BaFe_2As_2 below 8000 cm^{-1} . Inset: $R(\omega)$ below 50000 cm^{-1} . (b) $\sigma_1(\omega)$ below 10000 cm^{-1} (together with the low- ω extrapolation based on the dc conductivity). Inset: $\sigma_1(\omega)$ below 20000 cm^{-1} ($T=300 \text{ K}$), the intra- and interband terms, and the mid-infrared peak from the Drude-Lorentz fit. (c) The spectral weight below 10000 cm^{-1} . Inset: the spectral weight up to 50000 cm^{-1} .

around 2000 cm^{-1} for 10 K . Then the T -dependent suppression before the mid-infrared peak results in the second spectral weight suppression at 10 K near 3000 cm^{-1} . The lost weight finally recovers at about 8000 cm^{-1} . We would like to emphasize that this gap-like feature is not directly related to the SDW order. This is because (1) the mid-infrared suppression feature is present above T_{SDW} , (2) similar features exist for K - or Co -doped superconducting samples where the SDW order and the associated low energy gap structures are completely absent,[28] and (3) the energy scale is much larger than the SDW gaps. Usually a gap formation is associated with a broken symmetry state. As the AFe_2As_2 compounds are in their paramagnetic phase with a tetragonal crystal structure above T_{SDW} , both magnetic and crystal structures are in very high symmetry state, one would hardly expect an even higher magnetic or crystal structural symmetry at higher temperatures. Definitely, further experimental and theoretical works are necessary to understand this high energy gap-like behavior.

To summarize, the *ab*-plane optical measurements of AFe_2As_2 ($A=\text{Ba}, \text{Sr}$) single crystals were performed. For the SDW state, our findings indicate the Fermi surface is largely affected by the SDW transition. Based on a Drude-Lorentz model, we estimate that about 88% itinerant carriers were removed by the gapping of Fermi surfaces. Meanwhile, the carrier scattering rate was reduced by 92-96%. More importantly, we find two distinct gaps in the SDW ordered state in AFe_2As_2 . For the high frequency regions, $R(\omega)$ show anomalous T dependence even above T_{SDW} near the 5000 cm^{-1} mid-infrared component, which suggests the role of $\text{Fe } 3d$ electrons in AFe_2As_2 system might be very complex and unusual. Since AFe_2As_2 ($A=\text{Ba}, \text{Sr}$) systems have rather high conducting carrier density at high T , a driving mechanism based on an itinerant picture for the SDW instability is thus favored.

This work is supported by the National Science Foundation of China, the Knowledge Innovation Project of

the Chinese Academy of Sciences, and the 973 project of the Ministry of Science and Technology of China.

-
- [1] Y. Kamihara, T. Watanabe, M. Hirano, and H. Hosono, *J. Am. Chem. Soc.* **130**, 3296 (2008).
 - [2] G. F. Chen, Z. Li, D. Wu, G. Li, W. Z. Hu, J. Dong, P. Zheng, J. L. Luo, and N. L. Wang, *Phys. Rev. Lett.* **100**, 247002 (2008).
 - [3] X. H. Chen, T. Wu, G. Wu, R. H. Liu, H. Chen, and D. F. Fang, *Nature* **453**, 761 (2008).
 - [4] Z. A. Ren, W. Lu, J. Yang, W. Yi, X. L. Shen, Z. C. Li, G. C. Che, X. L. Dong, L. L. Sun, F. Zhou, Z. X. Zhao, *Chin. Phys. Lett.* **25**, 2215 (2008)
 - [5] J. Dong, H. J. Zhang, G. Xu, Z. Li, G. Li, W. Z. Hu, D. Wu, G. F. Chen, X. Dai, J. L. Luo, Z. Fang, N. L. Wang, *Europhys. Lett.* **83**, 27006 (2008).
 - [6] C. de la Cruz, Q. Huang, J. W. Lynn, J. Li, W. R. Li, J. L. Zarestky, H. A. Mook, G. F. Chen, J. L. Luo, N. L. Wang, and P. Dai, *Nature* **453**, 899 (2008).
 - [7] T. Yildirim, *Phys. Rev. Lett.* **101**, 057010 (2008).
 - [8] Q. Si, E. Abrahams, *Phys. Rev. Lett.* **101**, 076401 (2008).
 - [9] F. Ma, Z.Y. Lu, and T. Xiang, arXiv:0804.3370 (2008).
 - [10] C. Fang, H. Yao, W.-F. Tsai, J. Hu, S. A. Kivelson, *Phys. Rev. B* **77**, 224509 (2008).
 - [11] Cenke Xu, Markus Mueller, Subir Sachdev, *Phys. Rev. B* **78**, 020501(R) (2008).
 - [12] J. Wu, P. Phillips and A. H. Castro Neto, *Phys. Rev. Lett.* **101**, 126401 (2008).
 - [13] I.I. Mazin, M.D. Johannes, L. Boeri, K. Koepernik, D.J. Singh, arXiv:0806.1869
 - [14] M. Rotter, M. Tegel, D. Johrendt I. Schellenberg, W. Hermes, R.Pottgen, *Phys. Rev. B* **78**, 020503(R) (2008).
 - [15] M. Rotter, M. Tegel, D. Johrendt, *Phys. Rev. Lett.* **101**, 107006 (2008).
 - [16] C. Krellner, N. Caroca-Canales, A. Jesche, H. Rosner, A. Ormeci, C. Geibel, *Phys. Rev. B* **78**, 100504(R) (2008).
 - [17] G. F. Chen, Z. Li, G. Li, W. Z. Hu, J. Dong, P. Zheng, N. L. Wang and J. L. Luo, *Chin. Phys. Lett.* **25**, 3403 (2008).
 - [18] Q. Huang, Y. Qiu, Wei Bao, J.W. Lynn, M.A. Green, Y. Chen, T. Wu, G. Wu, X.H. Chen, arXiv:0806.2776.

- [19] Jun Zhao, W. Ratcliff II, J. W. Lynn, G. F. Chen, J. L. Luo, N. L. Wang, Jiangping Hu, Pengcheng Dai, Phys. Rev. B **78**, 140504(R) (2008).
- [20] N. Ni, S. L. Bud'ko, A. Kreyssig, S. Nandi, G. E. Rustan, A. I. Goldman, S. Gupta, J. D. Corbett, A. Kracher, P. C. Canfield, Phys. Rev. B **78**, 014507 (2008).
- [21] G. F. Chen, Z. Li, J. Dong, G. Li, W. Z. Hu, X. D. Zhang, X. H. Song, P. Zheng, N. L. Wang, J. L. Luo, arXiv:0806.2648.
- [22] L. Degiorgi, M. Dressel, A. Schwartz, B. Alavi, and G. Grüner, Phys. Rev. Lett. **76**, 3838 (1996).
- [23] V. Vescoli, L. Degiorgi, M. Dressel, A. Schwartz, W. Henderson, B. Alavi, G. Grüner, J. Brinckmann and A. Virosztek, Phys. Rev. B **60**, 8019 (1999).
- [24] M. A. Lind and J. L. Stanford, Phys. Lett. **39A**, 5 (1972).
- [25] L. X. Yang, Y. Zhang, H. W. Ou, J. F. Zhao, D. W. Shen, B. Zhou, J. Wei, F. Chen, M. Xu, C. He, Y. Chen, Z. D. Wang, X. F. Wang, T. Wu, G. Wu, X. H. Chen, M. Arita, K. Shimada, M. Taniguchi, Z. Y. Lu, T. Xiang, D. L. Feng, arXiv:0806.2627.
- [26] C. Liu, G. D. Samolyuk, Y. Lee, N. Ni, T. Kondo, A. F. Santander-Syro, S. L. Bud'ko, J. L. McChesney, E. Rotenberg, T. Valla, A. V. Fedorov, P. C. Canfield, B. N. Harmon, A. Kaminski, arXiv:0806.3453.
- [27] Suchitra E. Sebastian, J. Gillett, N. Harrison, P. H. C. Lau, D. J. Singh, C. H. Mielke, and G. G. Lonzarich, J. Phys.: Condens. Matter **20**, 422203 (2008).
- [28] G. Li, W. Z. Hu, J. Dong, Z. Li, P. Zheng, G. F. Chen, J. L. Luo, N. L. Wang, Phys. Rev. Lett. **101**, 107004 (2008).